Jefferson could possibly have illegitimately fathered an ancestor of the presumed male-line descendant of Eston. But in the absence of historical evidence to support such possibilities, we consider them to be unlikely.

Eugene A. Foster*, M. A. Jobling†, P. G. Taylor†, P. Donnelly‡, P. de Knijff§, Rene Mieremet§, T. Zerjal¶, C. Tyler-Smith¶

**6 Gildersleeve Wood, Charlottesville, Virginia 22903, USA*
e-mail: eafoster@aol.com
†Department of Genetics, University of Leicester, Adrian Building, University Road, Leicester LE1 7RH, UK
‡Department of Statistics, University of Oxford, South Parks Road, Oxford OX1 3TG, UK
§MGC Department of Human Genetics, Leiden University, PO Box 9503, 2300 RA Leiden, The Netherlands
¶Department of Biochemistry, University of Oxford, South Parks Road, Oxford OX1 3QU, UK

1. Peterson, M. D. *The Jefferson Image in the American Mind* 181–187 (Oxford Univ. Press, New York, 1960).
2. Malone, D. *Jefferson the President: First Term, 1801–1805* Appendix II, 494–498 (Little Brown, Boston, MA, 1970).
3. Brodie, F. M. *Thomas Jefferson: An Intimate History* (Norton, New York, 1974).
4. Ellis, J. J. *American Sphinx: The Character of Thomas Jefferson* (Knopf, New York, 1997).
5. Callender, J. T. *Richmond Recorder* 1 September 1802. [Cited in: Gordon-Reed, A. *Thomas Jefferson and Sally Hemings: An American Controversy* (Univ. Press of Virginia, Charlottesville, 1997)].
6. Woodson, M. S. *The Woodson Source Book* 2nd edn (Washington, 1984).
7. Hammer, M. F. *Mol. Biol. Evol.* **11,** 749–761 (1994).
8. Whitfield, L. S., Sulston, J. E. & Goodfellow, P. N. *Nature* **378,** 379–380 (1995).
9. Seielstad, M. T. *et al. Hum. Mol. Genet.* **3,** 2159–2161 (1994).
10. Zerjal, T. *et al. Am. J. Hum. Genet.* **60,** 1174–1183 (1997).
11. Mathias, N., Bayes, M. & Tyler-Smith, C. *Hum. Mol. Genet.* **3,** 115–123 (1994).
12. Kwok, C. *et al. J. Med. Genet.* **33,** 465–468 (1996).
13. Kayser, M. *et al. Int. J. Legal Med.* **110,** 125–133 (1997).
14. Jobling, M. A., Bouzekri, N. & Taylor, P. G. *Hum. Mol. Genet.* **7,** 643–653 (1998).

Coherent light scattering by blue feather barbs

The structural colours of avian feather barbs are created by the scattering of light from the spongy matrix of keratin and air in the medullary layer of the barbs[1–5]. However, the precise physical mechanism for the production of these colours is still controversial[1,3,4,6]. Here we use a two-dimensional (2D) Fourier analysis of the spatial variation in refractive index of the blue feather barbs of the plum-throated cotinga (*Cotinga maynana*, Cotingidae) to show that the colour is produced by constructive interference between light waves scattered coherently by the nanostructured keratin–air matrix of the barbs.

Mechanisms proposed to explain the production of structural colours of feather barbs fall into two classes, according to whether the vacuoles in medullary keratin scatter light coherently (with a relationship between the phases of waves scattered by different surfaces) or incoherently. In the Rayleigh and Mie scattering models[4,6], the colours are produced by incoherent scattering of smaller visible wavelengths by an array of spatially independent air vacuoles in the medullary keratin. Alternatively, in the constructive interference model, the colours are produced by interactions between light waves scattered coherently by the keratin–air matrix[1–3,5]. Out-of-phase waves will destructively interfere and cancel out, whereas in-phase waves will constructively reinforce one another and be reflected coherently. The phase relationships of scattered waves are determined by the size and spatial distribution of the scatterers[1,2,7]. Periodic spatial relationships between scatterers will produce consistent path-length differences among scattered waves and reinforce a limited set of wavelengths.

To investigate how the structural colour of feather barbs is produced, we apply an electromagnetic theory of coherent light scattering[7] that was developed to explain the transparency of the human cornea. In a quasi-random array of scatterers, coherent scattering is predicted only for light waves with a wavelength of twice that of the largest components of the Fourier transform of the spatial variation in refractive index[7]. We performed a discrete 2D Fourier analysis of digitized transmission electron micrographs of cross-sections of the medullary keratin from the blue feather barbs of *C. maynana* to examine whether it has periodic spatial variation in refractive index. The spongy medullary layer of *C. maynana* barbs consists of a matrix of keratin bars with air vacuoles of strikingly uniform diameter and spacing[2]. The matrix has no planes of symmetry and is randomly orientated to the surface of the feather. The 2D Fourier power spectrum of the medullary keratin matrix shows a nearly circular ring around the origin 0.0059 nm^{-1} in diameter (Fig. 1a). This ring indicates that the tissue has a highly ordered, nanoscale spatial variation in refractive index that is nearly uniform in all directions.

Reflection spectra of the blue feather barbs display a peak between 500 and 520 nanometres (Fig. 1b). We used the 2D Fourier power spectrum to predict the reflectance spectrum of these barbs. The

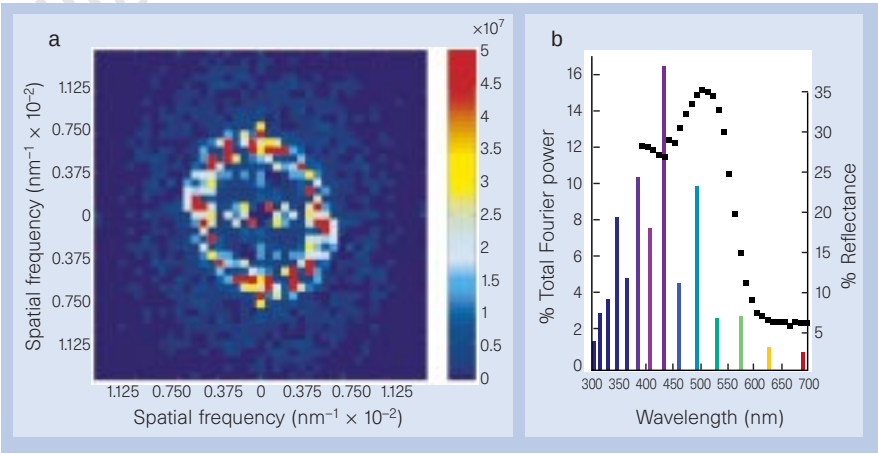

Figure 1 Two-dimensional Fourier power spectrum and observed and predicted reflectance spectra of a blue feather barb of *Cotinga maynana*. a, 2D Fourier power spectrum of the spongy medullary keratin matrix of a blue feather barb. b, Observed reflectance spectrum of a blue feather barb (black squares, right axis) and predicted reflectance spectrum (bars, left axis) based on the 2D Fourier power spectrum (a). The discrete Fourier transform describes how a signal or image is composed of different periodic component waves[10]. A 2D Fourier analysis was conducted using the 2D Fast Fourier Transform algorithm in MATLAB[11] on a digitized 500-$pixel^2$ image of a transmission electron micrograph (magnification, × 29,000)[2]. The image was processed in MATLAB using variance rescaling with block processing and median filtering[11]. The 2D Fourier power spectrum (a) resolves the spatial variation in optical density in the tissue into its periodic components in any direction in the plane from all points. The size and direction of any component spatial frequency is given by the length and direction of a vector from the origin to that point. The squared amplitude of the component is given by the colour (scale bar on the right). The ring indicates a highly ordered, nanoscale fluctuation in optical density moving in any direction in the plane of the tissue at a spatial frequency of about 0.0059 nm^{-1}. Reflectance of blue feather barbs (b, squares, right axis) was measured using a Zeiss microspectrophotometer at 30 wavelengths between 400 and 700 nm[12]. The predicted reflectance spectrum (b, bars, left axis) expresses the percentage of the total power distributed among the components of the 2D Fourier power spectrum over all directions. The predicted reflection spectrum was calculated using the radial average of one quadrant of the 2D Fourier power spectrum with half-pixel width intervals, normalizing the volume under the rotated radial average function to one, calculating the volume under radial sections of the radial average Fourier power function, multiplying these volumes by twice the mean refractive index (1.283), estimated from the micrographs using the refractive indices of keratin (1.54) and air (1.00)[2], and plotting these values as wavelengths in nanometres.

predicted reflectance spectrum shows a peak at 435 nanometres with descending slopes towards both ends of the visible spectrum (Fig. 1b), which agrees well with the observed reflectance spectrum in hue (position of peak) and chroma (shape of peak). Most of the total power in the Fourier power spectrum is concentrated at spatial frequencies that will produce coherent scattering of light waves that are close to the observed blue hue. The correspondence between the peaks of the observed and predicted reflection spectra (about 75 nanometres) is striking as there are no reasons, apart from structural colour production, to expect these spatial frequencies to predominate.

In the Mie and Rayleigh scattering models, the medullary keratin scatters incoherently (which means the scatterers must be separated by distances larger than the wavelength of visible light)[8]. However, the ring-like Fourier power spectrum demonstrates that the scatterers in medullary keratin are spatially periodic on a scale smaller than visible wavelengths, so scattering is coherent. Furthermore, the air vacuoles in the medullary keratin of *C. maynana* and other structurally coloured feather barbs[3,5] are too close together to scatter visible light incoherently. Finally, the Rayleigh model predicts that the reflectance spectrum should increase continuously into the ultraviolet[1], but the distinct peak in the reflection spectrum shows this prediction to be false (Fig. 1b). Rayleigh scattering has been the traditional explanation of this phenomenon for nearly a century[4], and remains widely cited in ornithological texts and reference works[9], but our results indicate that the Rayleigh model and other incoherent scattering models are not suitable explanations.

Our analysis of the spatial variation in the refractive index of medullary keratin shows that this tissue is a highly ordered nanostructure of the appropriate size to produce the observed hue by constructive interference. The similarity in nanostructure between the medullary keratin of *C. maynana* and other structurally coloured feather barbs indicates that constructive interference probably also causes the production of the structural greens, blues, violets and ultraviolet colours in other feather barbs[1–5].

Richard O. Prum*†, Rodolfo H. Torres‡, Scott Williamson†, Jan Dyck§

**Natural History Museum, and Departments of †Ecology and Evolutionary Biology, and ‡Mathematics, University of Kansas, Lawrence, Kansas 66045, USA*
e-mail: prum@ukans.edu
§Institute of Population Biology, Universitetsparken 15, DK-2100 Copenhagen, Denmark

1. Dyck, J. *Biol. Skrift.* **18,** 1–67 (1971).
2. Dyck, J. *Z. Zellforsch.* **115,** 17–29 (1971).
3. Dyck, J. *Proc. Int. Ornithol. Congr.* **16,** 426–437 (1976).
4. Fox, D. L. *Animal Biochromes and Structural Colors* (Univ. California Press, Berkeley, 1976).
5. Durrer, H. in *Biology of the Integument* Vol. 2. *Vertebrates* (eds Bereiter-Hahn, J., Matoltsky, A. G. & Richards, K. S.) 239–247 (Springer, Berlin, 1986).
6. Finger, E. *Naturwissenschaften* **82,** 570–573 (1995).
7. Benedek, G. B. *Appl. Optics* **10,** 459–473 (1971).
8. Bohren, C. F. & Huffman, D. R. *Absorption and Scattering of Light by Small Particles* (Wiley, New York, 1983).
9. Gill, F. B. *Ornithology* (Freeman, New York, 1995).
10. Briggs, W. L. & Henson, V. E. *The DFT* (Society for Industrial and Applied Mathematics, Philadelphia, 1995).
11. *MATLAB Reference Guide* (Mathworks, Natick, MA, 1992).
12. Dyck, J. *Anser* (suppl.) **3,** 57–75 (1978).

A lower jaw from a Cretaceous parrot

All known Cretaceous bird fossils representing modern higher taxa are from the aquatic groups Anseriformes[1–3], Gaviiformes[4,5], Procellariiformes[1] and Charadriiformes[1,6]. Here I describe a toothless avian dentary symphysis (fused jawbone) from the latest Cretaceous of Wyoming, United States. This symphysis appears to represent the oldest known parrot and is, to my knowledge, the first known fossil of a 'terrestrial' modern bird group from the Cretaceous. The existence of this fossil supports the hypothesis, based on molecular divergence data[7,8], that most or all of the major modern bird groups were present in the Cretaceous.

The specimen (Fig. 1) is from UCMP locality V65238 in the Lance Formation, Lancian North American Land Mammal Age, Maastrichtian, latest Cretaceous, Niobrara County, Wyoming. The mandibular symphysis is deeply concave, with a nearly U-shaped cross-section at the posterior end of the fragment, and has a rounded anterior margin (Fig. 1). The left and right dentaries are fused completely without a suture. Small bone fibres indicate that the individual was at or close to adult size, so the characters are not juvenile states. The labial surface of the mandibular symphysis has a highly vascularized appearance, produced by numerous foramina (openings), canals and grooves for neurovascular tissue (Fig. 1c), like those present in the area in which a horny covering, or rhamphotheca, is attached to the jaw in living amniotes.

A completely fused and edentulous (toothless) mandibular symphysis is present only in turtles, oviraptorids, ornithomimids, caenagnathid theropods and neornithine birds. The pair of lingual median symphysial foramina next to the sagittal plane is found in most neornithines, including Anseriformes, Galliformes, Psittaciformes and other orders, but is absent in hesperornithiforms, oviraptorids and turtles. Caenagnathid theropods have lateral grooves, lateral occlusal grooves, lingual ridges, longitudinal vascular grooves, meckelian grooves and median tubercles[9], which

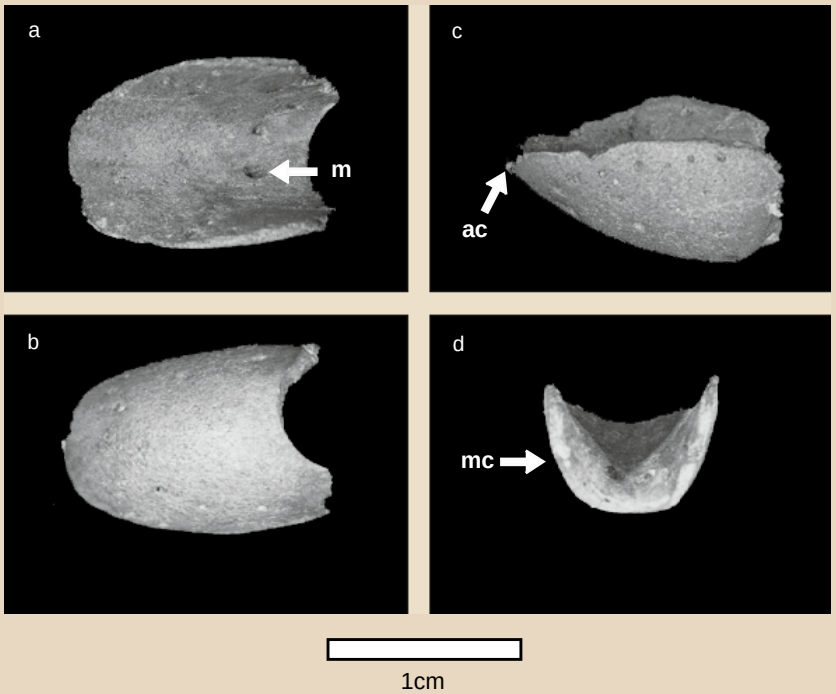

Figure 1 Mandibular symphysis of the Lance Formation parrot (University of California Museum of Paleontology, specimen UCMP 143274). a, Dorsal view. The two large median foramina (m) on the lingual surface 3.0 millimetres from the posteroventral edge of the symphysis are equidistant from the midline, with very short grooves posterior to them. b, Ventral view. c, Dorsolateral view, showing anterior accessory canal opening (ac) and large labial foramina; the right tomial crest is slightly concave, curving ventrally, and the left is worn and does not have a concave dorsal margin. d, Posterior view, showing meckelian canal (mc). Anterior is to the left in a–c.